Progress Report

CART Raman Lidar Measurements of Atmospheric Aerosols for the Atmospheric Radiation Measurement (ARM) Program

Dr. Richard A. Ferrare (PI)
NASA Langley Research Center
Mail Stop 401A
Hampton, Virginia 23681
757-864-9443; 757-864-7790 (fax)
r.ferrare@larc.nasa.gov

David D. Turner (Co-I)
Pacific Northwest National Lab
P.O. Box 999, MSIN K9-24
Richland, Washington 99352
509-375-2590; 509-372-6247 (fax)
dd_turner@pnl.gov

Dr. Tim Tooman (Co-I)
Sandia National Laboratories
P.O. Box 969, MS 9056
Livermore, CA 94551-0969
510-294-2752; 510-294-1559 (fax)
tooman@ca.sandia.gov

Scientific Goals

Vertical profiles of aerosol extinction are required for determination of the effects of aerosols on the clear-sky radiative flux. We are developing, evaluating, and implementing algorithms for the CART Raman lidar to provide profiles of aerosol extinction and backscattering. We are using these profiles to characterize the vertical distribution of aerosol scattering and extinction above the SGP site, and how these distributions vary with time. These aerosol extinction profiles are integrated with altitude to derive aerosol optical thickness to provide a nearly continuous record of this important aerosol parameter. Since the aerosol extinction/backscatter ratio depends on aerosol size and composition, an objective of this research is to evaluate the vertical and temporal variabilities in this parameter and determine how the aerosol extinction/backscatter is related to the aerosol size distribution and aerosol refractive index. By virtue of its ability to

measure vertical profiles of both aerosol extinction and water vapor simultaneously in the same scattering volume, we are also using the resulting profiles from the CART Raman lidar to investigate the impact of water vapor and relative humidity on aerosol extinction throughout the column on a continuous and routine basis. We are also investigating the relationship between vertical profiles of aerosol extinction and backscattering measured by the CART Raman Lidar with the aerosol physical and optical properties measured by other instruments. Another objective of this research is to develop Value-Added Procedures (VAPs), which are automatic algorithms running in the ARM Experiment Center to produce second generation data streams, to produce a “best-estimate” product to characterize the clear sky atmospheric state over the SGP site.

Special Accomplishments

- We have combined the aerosol and water vapor profiles from the Raman lidar and temperature profiles from AERI+GOES retrievals into a single “best estimate” (BE) VAP that takes advantage of both active and passive remote sensors to characterize the clear sky atmospheric state above the CART site. This BE VAP has also been implemented to run routinely at the ARM Experiment Center.
- We have used the profiles of aerosol backscattering and extinction from the SGP CART Raman lidar to characterize the vertical distribution of aerosols and optical thickness over the SGP during 1998 and 1999. The vertical distribution of aerosol extinction was found to differ between winter and summer in contrast to the vertical distribution of water vapor, which remained constant throughout the year.
- The Raman lidar measurements of the aerosol extinction/backscattering ratio were linearly correlated with the aerosol accumulation mode volume median radius and the ratio of accumulation/coarse particles.
- During about 20% of the time, there were significant variations in the vertical profile of the aerosol extinction/backscatter ratio, and consequently in the aerosol size distribution and/or composition.
- The Raman lidar measurements of aerosol extinction and relative humidity were used to investigate and parameterize how aerosol extinction increases with relative humidity near the top of the daytime boundary layer.

Progress and Accomplishments

We have developed a series of Value Added Procedures (VAPs) to use the CART Raman lidar data to routinely produce several data sets for use in characterizing the clear-sky state over the SGP site. These VAPs were implemented to run routinely at the U.S. Department of Energy's Atmospheric Radiation Measurement (ARM) Experiment Center. The output products from these VAPs included a series of netCDF files that include the profile results as well as several quick look GIF images to show the results of this processing. These VAPS include:

- MR VAP (water vapor mixing ratio and relative humidity profiles)
- ASR VAP (aerosol scattering ratio and backscatter coefficient profiles)
- EXT VAP (aerosol extinction coefficient and extinction/backscatter ratio)
- DEP VAP (depolarization and cloud mask profiles).

Automated algorithms to derive aerosol scattering ratio, backscattering, and extinction profiles from the SGP CART Raman lidar data were recently upgraded to improve performance during conditions of low aerosol loading. The corresponding VAPs discussed above were also updated at the ARM Experiment Center. These aerosol and water vapor profiles (Raman lidar) and temperature profiles (AERI+GOES) have been combined into a single "best estimate" (BE) VAP that takes advantage of both active and passive remote sensors to characterize the clear sky atmospheric state above the CART site. The products included in this BE VAP are profiles of water vapor mixing ratio, relative humidity, aerosol backscatter coefficient (at 355 nm), aerosol extinction coefficient (at 355 nm), temperature (from AERI+GOES retrievals), potential temperature (from AERI+GOES retrievals), total precipitable water vapor, aerosol optical thickness (at 355 nm), linear depolarization ratio, cloud mask. The characteristics of these products are listed in **Table 1.** This BE VAP has also been implemented to run routinely at the

ARM Experiment Center. The "best estimate" algorithms have been used to derive profiles for the following periods September 1996 (Water Vapor IOP #1), September-October 1997 (Water Vapor IOP#2, Aerosol IOP), April 1998 through present (June 2000). A web site showing these results for the periods listed above has been established at http://yard.arm.gov/~turner/raman_lidar_quicklooks.html. **Figure 1** shows examples of these images for a single day (December 3, 1998). These files are also available from the ARM archive (http://www.archive.arm.gov/data/ordering.html). Best estimate products are being produced on a routine basis by automated software at the DOE ARM Experiment Center. These data are also available from the ARM Archive.

As part of the routine diagnostics, the CART Raman Lidar (CARL) water vapor mixing ratio profiles were compared with water vapor profiles measured by Vaisala radiosondes launched at the SGP site. Over 500 lidar/radiosonde profile comparisons examined between April 1998 and October 1999 showed that the unscaled radiosondes were about 3-5% drier than the lidar. When the radiosonde water vapor mixing ratio was scaled to match the microwave precipitable water vapor amount, the scaled radiosonde and lidar water vapor profiles agreed generally within 1-2%. **Figure 2** shows these results. The AERI+Model temperature profiles were also compared with temperature profiles measured by Vaisala radiosondes. Over 450 AERI+model/radiosonde profile comparisons showed that rms temperature differences were less than 1 K, with the AERI+Model slightly (~0.25 K) warmer. **Figure 3** shows the comparison.

Aerosol optical thicknesses (AOT), which are computed by integrating the Raman lidar aerosol extinction profiles between 0-6 km, have been compared with simultaneous and independent measurements of AOT made by a Cimel sun photometer at the SGP CART site (**Figure 4**). The lidar and sun photometer AOT values generally agree, with about a 5% bias difference. Of this

difference, 3.5% can be explained by the wavelength dependence of aerosol extinction between the two wavelengths (340 nm vs. 355 nm). The CARL AOT also generally show good agreement with the Cimel AOT when compared as a function of season (**Figure 5**).

The Raman lidar aerosol extinction, water vapor, and relative humidity profiles have been used to examine the vertical variability of aerosols and water vapor. **Figure 6** shows the average aerosol extinction profiles for various ranges of AOT for data acquired between April 1998 to January 2000. The solid points on this graph indicate the scale height of the aerosols. **Figures 7** and **8** show the same for water vapor mixing ratio and relative humidity. The aerosol scale height was between 1.0-1.2 km during the winter but rose to nearly 2 km in the summer. This behavior is in contrast to the scale height for water vapor mixing ratio, which remained nearly the same (2.0-2.5 km) during winter and summer. The CARL aerosol extinction profiles also show that considerable aerosol loading often existed in elevated layer above the boundary layer. **Figure 9** shows an example when smoke from fires in Central America were observed over the ARM SGP CART site. Of particular importance in this case is the profile of the aerosol extinction/backscatter ratio (S_a) derived from the CARL data and which is also shown in this figure. Since S_a varies with changes in the aerosol size distribution and/or aerosol composition, variations in the vertical profile of S_a indicate that the aerosol size distribution and/or aerosol composition varied with altitude. In this example, the value of $S_a = 55$ sr observed for the boundary layer aerosols is typical of the aerosols observed over the SGP site. In contrast, the value of $S_a = 90$ sr observed for the elevated aerosol layer between 3-6 km is typical for biomass burning aerosols. We used aerosol size distributions derived from the Cimel Sun photometer sun and sky radiance measurements to show that the biomass burning aerosols are consistent with the CARL S_a measurements. We examined the aerosol extinction/backscattering profiles derived

from the CARL measurements to determine the how often aerosol optical and physical characteristics vary with altitude as in the case described above. In this study, we computed the standard deviation (due to atmospheric variability) of S_a in a vertical column. For cases when the AOT at 355 nm was greater than 0.3, **Figure 10** shows that, for data acquired between April 1998 and April 1999, in about 20% of the cases the standard deviation of S_a due to atmospheric variability was greater than 10 sr (or 15%). This type of variability is similar to that shown in **Figure 9** for the smoke aerosols. In these cases of high S_a variability, the aerosol size distribution and/or composition varied significantly with altitude. These results suggest that column averages may not accurately represent the true aerosol characteristics in a significant number of cases.

The CARL retrievals of S_a were compared with the aerosol size parameters derived from coincident sun and sky radiance data measured by a Cimel Sun photometer data. An inversion procedure, which has been developed by Oleg Dubovik at NASA/GSFC, uses the Cimel direct solar and the sky brightness measurements to derive column-averaged aerosol size distribution, complex refractive index, and single scattering albedo, as well as the aerosol extinction/backscatter ratio. **Figure 11** shows a comparison of the CARL and Cimel S_a values as well as how these values vary with wavelength. **Figure 12** shows that the CARL S_a values are linearly correlated with the fine (accumulation) mode volume median radius as well as the volume ratio (fine/coarse). This shows that the CARL S_a measurements may be used to indicate particle sizes.

The CARL data have also been used to investigate how aerosol extinction and the aerosol extinction/backscatter ratio vary with relative humidity. **Figure 13** shows an example of how CARL data have been used to observe the increase in aerosol extinction with relative humidity

near the top of the daytime boundary layer. We have examined measurements from several of these days to show the dependence of aerosol extinction and S_a on relative humidity. **Figure 14** shows that the ratio of aerosol extinction at RH=80% to that at RH=30% is about 1.9 +/- 0.4 which is not inconsistent with the values derived from the SGP surface in situ measurements. The increase in S_a with relative humidity also shown in **Figure 14** is consistent with that modeled for “continental aerosols”.

Refereed Publications

Automated retrievals of aerosol extinction and backscatter coefficient profiles from a Raman lidar. D.D. Turner, R.A. Ferrare, L.A. Heilman, W.F. Feltz, and T.P. Tooman. Journal of Applied Meteorology, submitted, 2000.

ARM Southern Great Plains observations of the smoke pall associated with the 1998 Central American fires. R.A. Peppler, L. Ashford, C.P. Bahrmann, J.C. Barnard, R.A. Ferrare, R.N. Halthore, N.S. Laulainen, J.A. Ogren, M.R. Poellot, M.E. Splitt, and D.D. Turner. Bulletin of the American Meteorological Society, in press, 2000.

A comparison of the aerosol optical thickness derived from ground-based and airborne measurements. S. Kato, M.H. Bergin, T.P. Ackerman, T.P. Charlock, E.E. Clothiaux, R.A. Ferrare, R.N. Halthore, N. Laulainen, G.G. Mace, J. Michalsky, and D.D. Turner. Journal of Geophysical Research, J. Geophys. Res., 105, No. D11, 14701-14717, 2000.

Continuous water vapor profiles from operational active and passive remote sensors. D.D. Turner, W.F. Feltz, and R.A. Ferrare. Bulletin of the American Meteorological Society, 81, 1301-1317, 2000.

Extended Abstracts

"CART Raman Lidar Retrievals of Aerosol Extinction and Relative Humidity Profiles", D.D. Turner, R.A. Ferrare, L.A. Heilman, W.F. Feltz, 10th Conference on Atmospheric Radiation, American Meteorological Society, June 28-July 2, 1999, Madison, Wisconsin, 434-437.

"Raman Lidar Profiling of Water Vapor and Aerosols over the ARM SGP Site", R.A. Ferrare, D.D. Turner, L.A. Heilman, W.F. Feltz, R.A. Peppler, T. Tooman, and R. Halthore, Symposium on Lidar Atmospheric Monitoring, American Meteorological Society, American Meteorological Society, January 9-14, 2000, 1-4.

"Characterization of the Atmospheric State above the SGP Using Raman Lidar and AERI/GOES Measurements", R.A. Ferrare, D.D. Turner, L.A. Heilman, W.F. Feltz, T. Tooman, O. Dubovik, R. Halthore, Tenth ARM Science Team Meeting, San Antonio, Texas, March 13-17, 2000, (http://www.arm.gov/docs/documents/technical/conf_0003/ferrare-ra.pdf)

"Simultaneous Ground-Based Remote Sensing of Water Vapor by Differential Absorption and Raman Lidars", D. D. Turner, H. Linné, J. Bösenberg, S. Lehmann, K. Ertel, J. E. M. Goldsmith and T. P. Tooman, Tenth ARM Science Team Meeting, San Antonio, Texas, March 13-17, 2000, (http://www.arm.gov/docs/documents/technical/conf_0003/turner-dd.pdf)

"A Two Year Climatology of Water Vapor and Aerosols in the Lower Troposphere Measured by a Raman Lidar", D. D. Turner, R.A. Ferrare, L.A. Heilman, T.P. Tooman, 20th International Laser Radar Conference, Vichy, France, July 10-14, 2000.

Proposed work for one year renewal

As part of our efforts to develop a “best estimate” product to characterize the atmospheric state above the SGP site, we have Value Added Procedure (VAP) to compute water vapor mixing ratio, relative humidity, and precipitable water vapor over the SGP site using data from both the Raman lidar and the AERI+GOES retrievals. We propose to investigate the distribution of relative humidity in the upper troposphere using these data. Accurate measurements of upper tropospheric relative humidity are important for initializing numerical weather models, computing shortwave and longwave radiation fluxes and cooling rates, forecasting the formation of aircraft contrails, and understanding and modeling ice nucleation in cirrus clouds. Predicting the formation and persistence of cirrus clouds in particular requires accurate measurements of ice supersaturation at high altitudes and corresponding cold temperatures. Recent measurements by in situ sensors on radiosondes and aircraft have shown that large ice supersaturations may exist at low temperatures in both clear and cloudy conditions. Since ice supersaturation often occurs in thin layers, the fraction of the upper troposphere where supersaturation exists may be considerably larger than deduced from in situ measurements, which suggests that the fraction of sky covered by optically thin cirrus clouds in moderately supersaturated regions can be large. We shall use these profiles of relative humidity acquired during nighttime operations of the Raman lidar to determine the frequency of occurrence of ice supersaturation conditions and relate these measurements to the occurrence of cirrus clouds.

We also propose to continue to investigate the relationship between vertical profiles of aerosol extinction and backscattering measured by the CART Raman lidar with the aerosol physical and optical properties measured by other instruments. Recently, a program was started to measure aerosol scattering and absorption properties in situ using instruments on board a light

aircraft. These flights, which are to occur on a routine basis 2-3 times per week, began in March 2000. The measurements are intended to address how aerosol properties vary through the column and under what conditions the surface measurements can be use to calculate radiative forcing (see http://www.cmdl.noaa.gov/aero/net/iap/). These measurements will also be useful for relating in situ measurements of aerosol scattering and absorption to the lidar measurements of aerosol backscattering and extinction. Since lidar systems are presently the only means of automatically and routinely monitoring the vertical distribution of aerosols, it is important to assess the ability of the lidar profiles to measure aerosol optical properties. At present, the only means of routinely assessing the lidar aerosol measurements is by comparing the aerosol optical thickness, which is found by integrating the aerosol extinction profile, with Sun photometer measurements. Since this compares only column-integrated measurements, it does not provide a means to evaluate the vertical structure of the aerosol profile. Comparing the lidar profiles with the aircraft measurements, and comparing both measurements with simultaneous Sun photometer measurements, would permit assessments of both the lidar and aircraft measurements. We would also use the Raman lidar measurements of aerosol extinction profiles to determine how much aerosol extinction and optical thickness is above the light aircraft maximum sampling altitude of about 3.5 km. To help facilitate this work, we would work toward the development of a VAP to combine the Raman lidar, light aircraft, and Sun photometer measurements.

Table 1. CART Raman Lidar/AERI+Model Clear-Sky Product Parameters

Measurement	Altitude Range	Vertical Resolution	Nominal Temporal Resol-ution	Error	Precision	Detection Limit
Aerosol Backscattering (355 nm)	0.060-8 km	78 m	10 min	5-10%	2%	0.0002-0.0004 km-sr^{-1}
Aerosol Extinction (355 nm)	0.1-8 km	150 m-1 km	10 min	5-10%	5%	0.02-0.03 km^{-1}
Aerosol Optical Thickness (355 nm)	-	-	10 min	5% or 0.03	5%	0.03
Water Vapor Mixing Ratio	0.060-8 km (night) 0.060-4 km (day)	78 m	2-10 min	5%	2%	0.002 g/kg
Relative Humidity	0.060-8 km (night) 0.060-4 km (day)	78 m	2-10 min	5%	5%	1%
Precipitable Water Vapor	-	-	10 min	5%	5%	2 mm
Linear Depolarization	1-14 km	39 m	1-10 min	10%	2%	
Temperature (AERI+Model)	0-3 km (AERI) 3-15 (Model)	100 m - 1 km	8 min	1 K	1 K	
Cloud Base Height	0.060-14 km	78 m	1-10 min	78 m	39 m	0.060 km

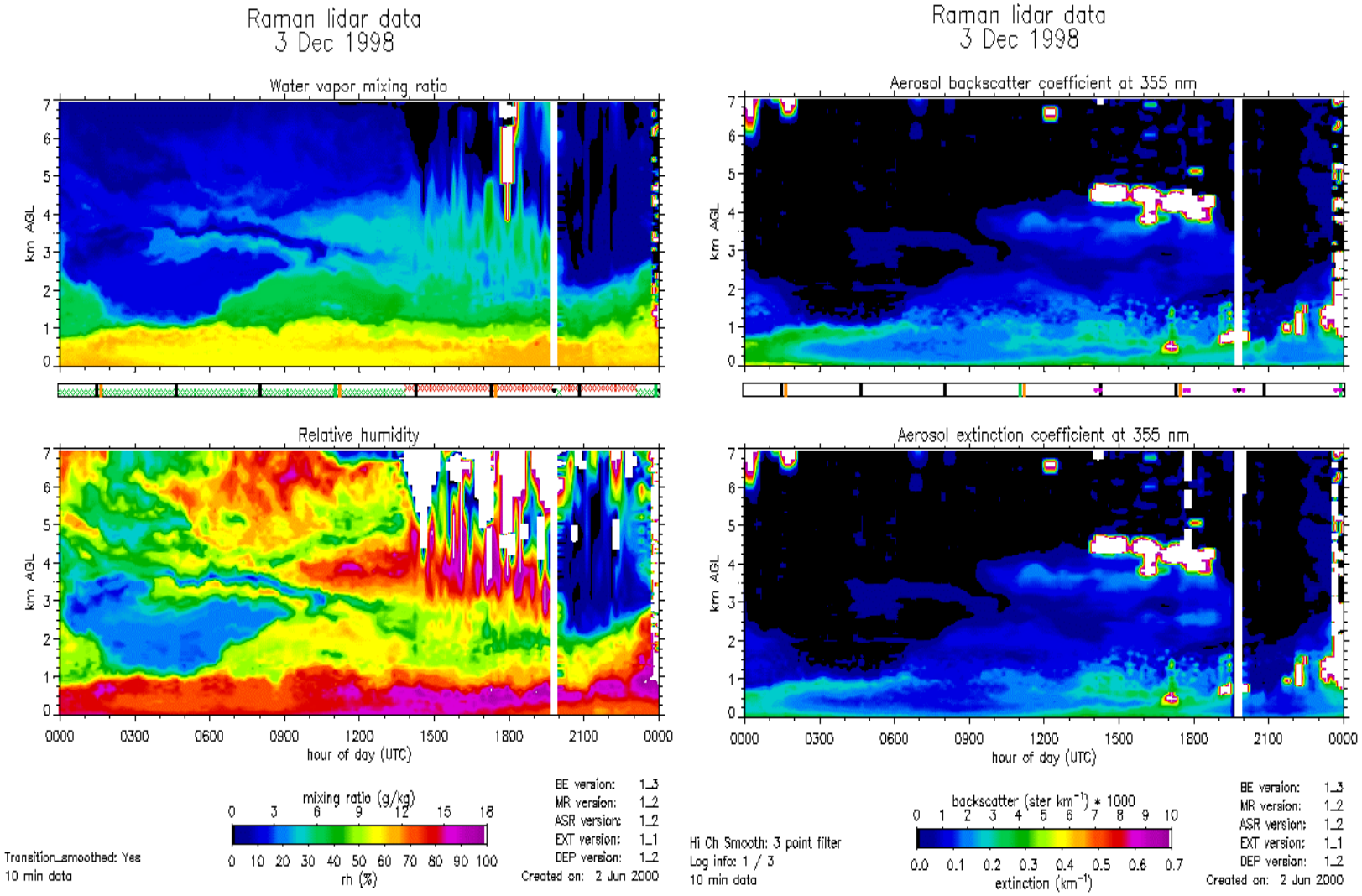

Figure 1. Example of CART Raman lidar water vapor (left) and aerosol (right) “quicklook” images for December 3, 1998.

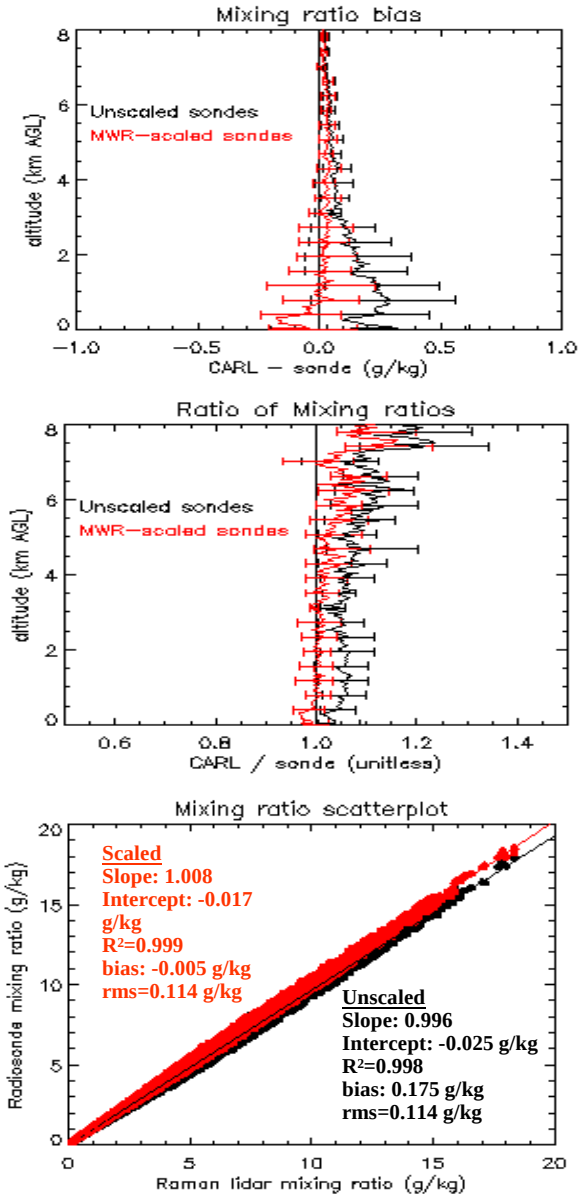

Figure 2. Comparison of CART Raman lidar and Vaisala radiosonde water vapor profile measurements.

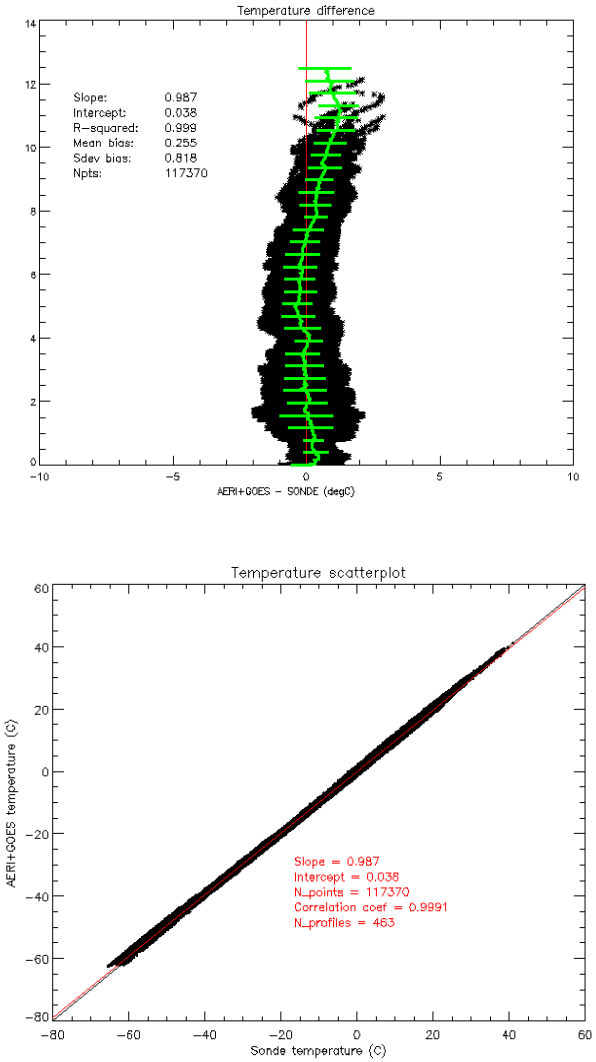

Figure 3. Comparison of AERI+Mode and radiosonde temperature profile measurements.

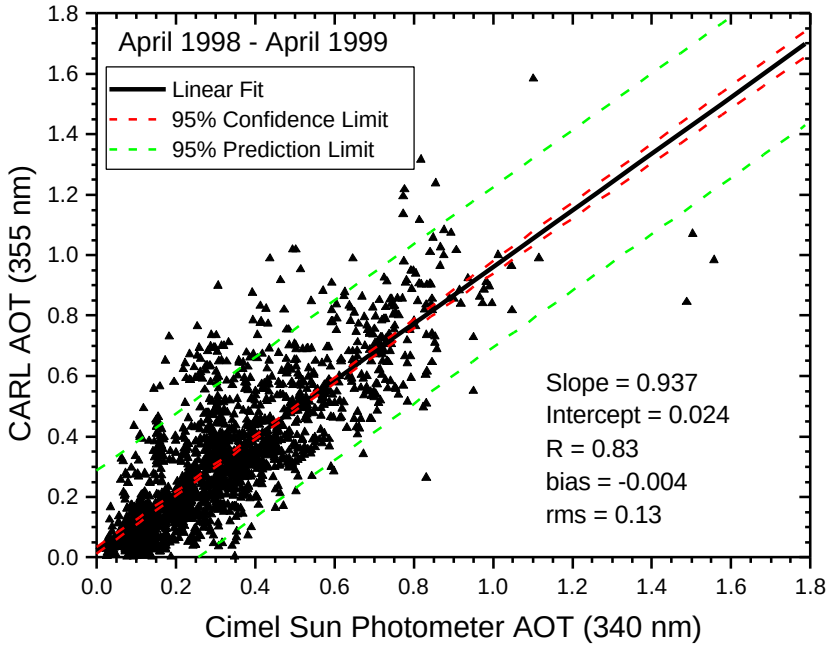

Figure 4. Comparison of AOT measured by Cimel Sun photometer and Raman lidar.

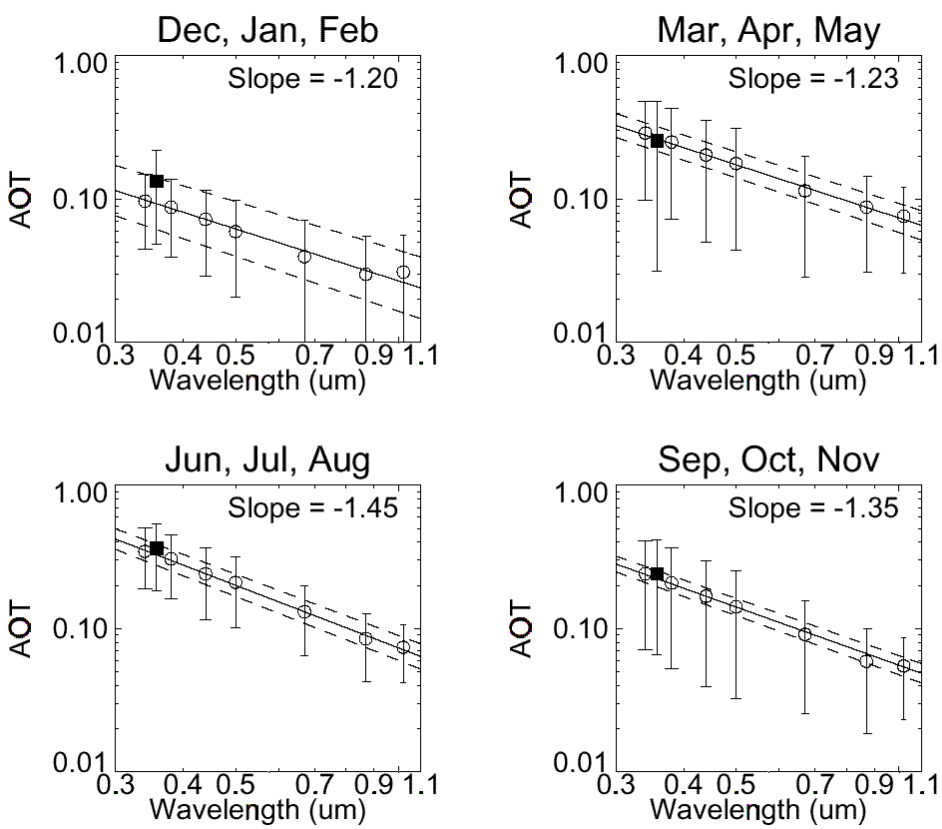

Figure 5. Comparisons of mean AOT from coincident samples from the CIMEL (open circles) and Raman lidar (solid squares) as a function of season. These are log-log plots. There were 225, 571, 562, and 1127 cloud-screened comparisons in the winter, spring, summer, and fall seasons, respectively. The solid lines represent the mean wavelength relationship, while the dotted lines are three times the standard deviation about this mean.

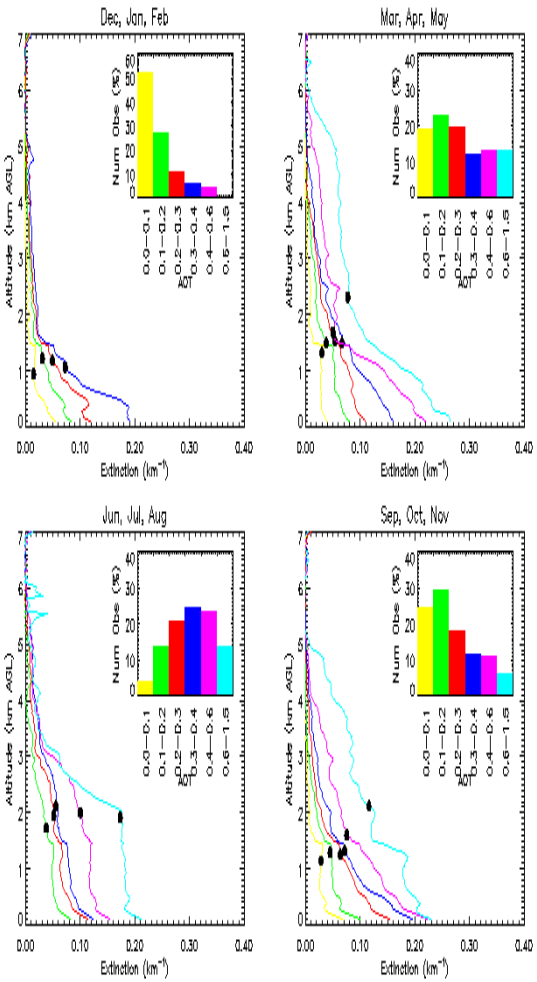

Figure 6. Mean extinction profiles as a function of aerosol optical thickness (AOT) and season for data from April 1998 – January 2000. The inset histograms indicate the distribution of the samples as a function of AOT bin for each season.

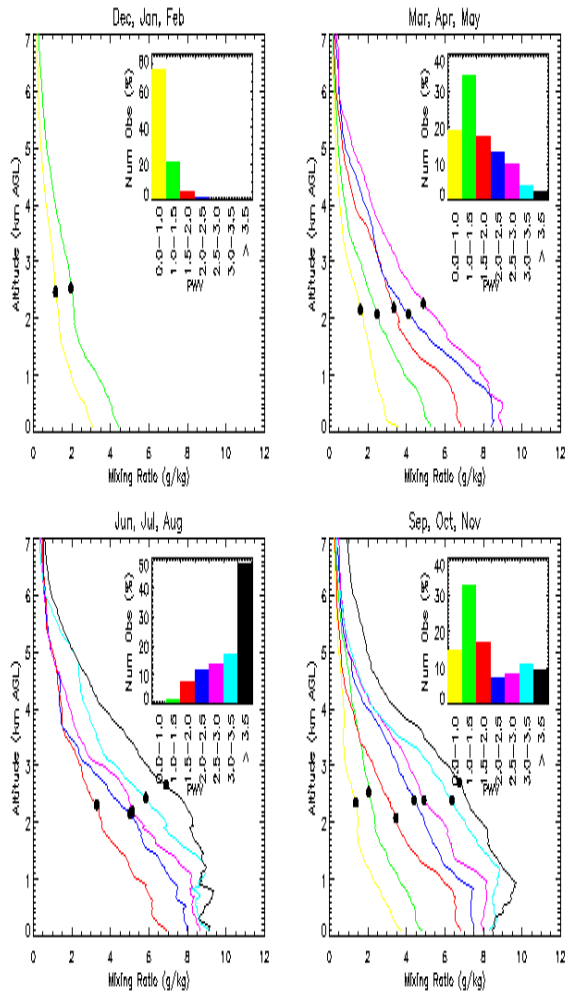

Figure 7. Mean water vapor mixing ratio profiles as a function of season and total precipitable water vapor for data from April 1998 – January 2000. The inset histograms indicate the distribution of the samples as a function of PWV for each season.

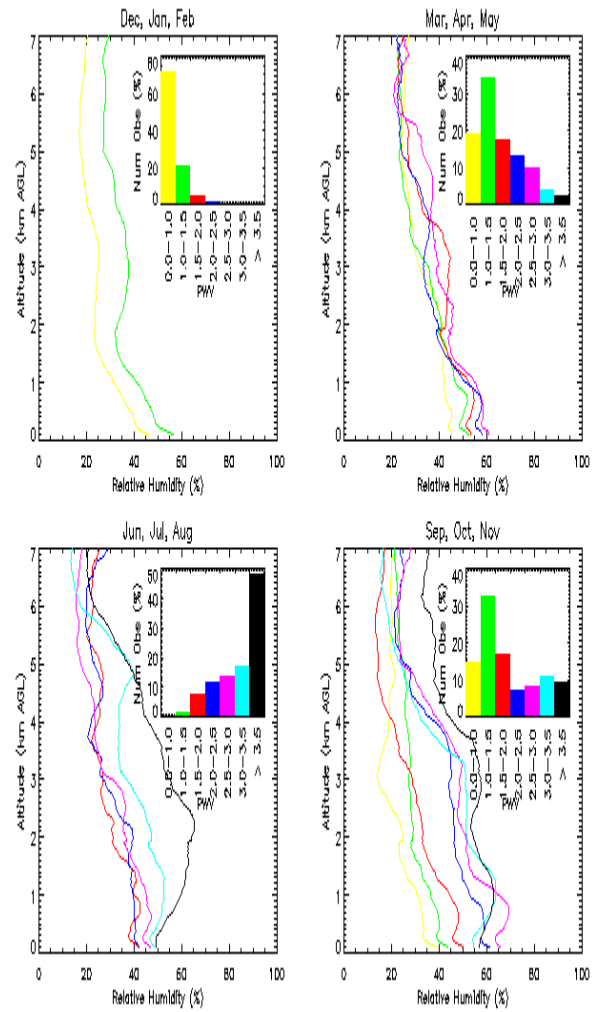

Figure 8. Same as figure 7, except these are mean relative humidity profiles instead of mean mixing ratio profiles.

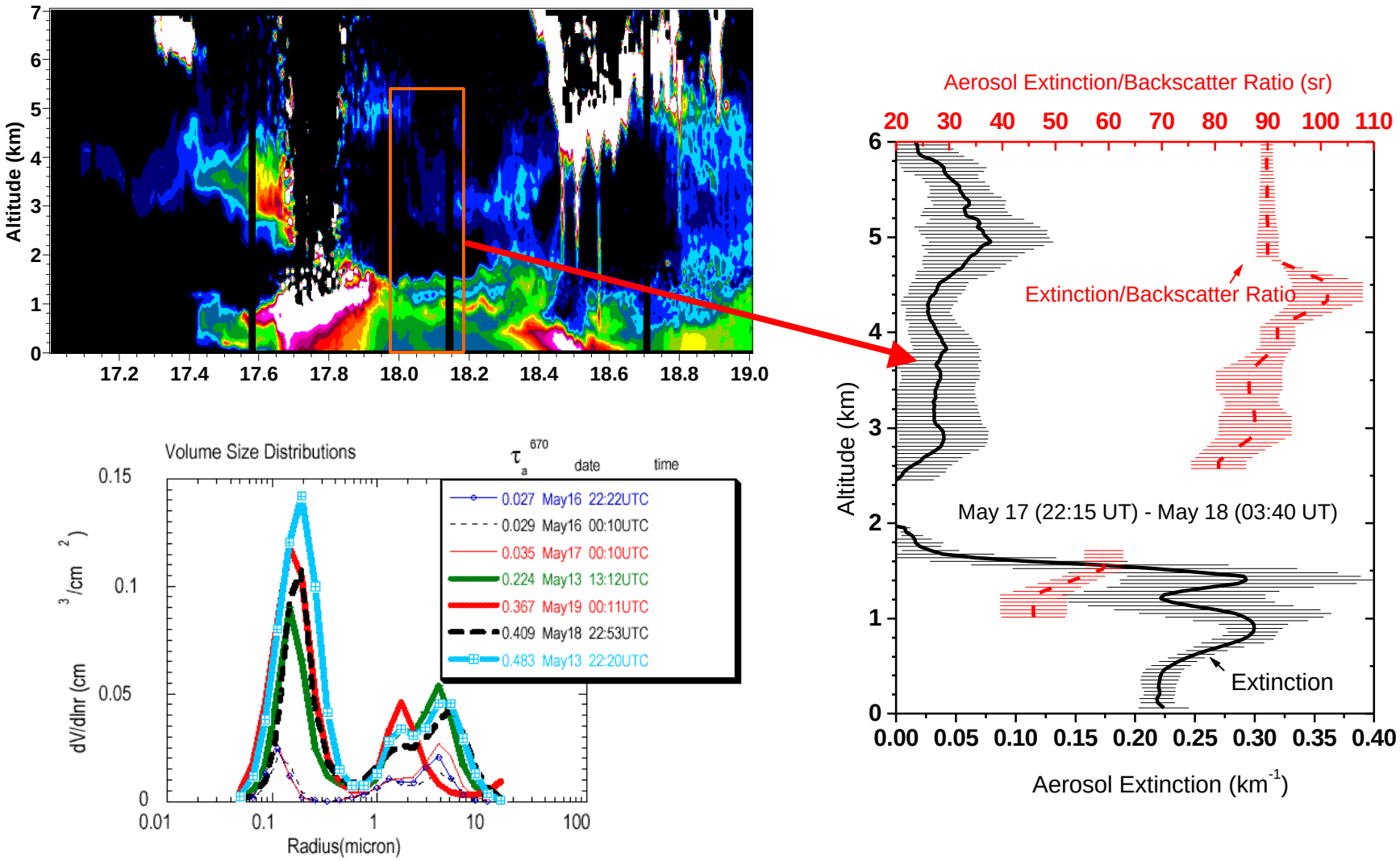

Figure 9 (top left) Image showing CART Raman lidar aerosol extinction profiles acquired on May 17-18, 1998. (right) CART Raman lidar profiles of aerosol extinction and aerosol extinction/backscattering ratio between 22:15 UT May 17 and 03:40 UT May 18. (bottom left) Aerosol volume size distribution derived from Cimel Sun photometer measurements of Sun and sky radiances.

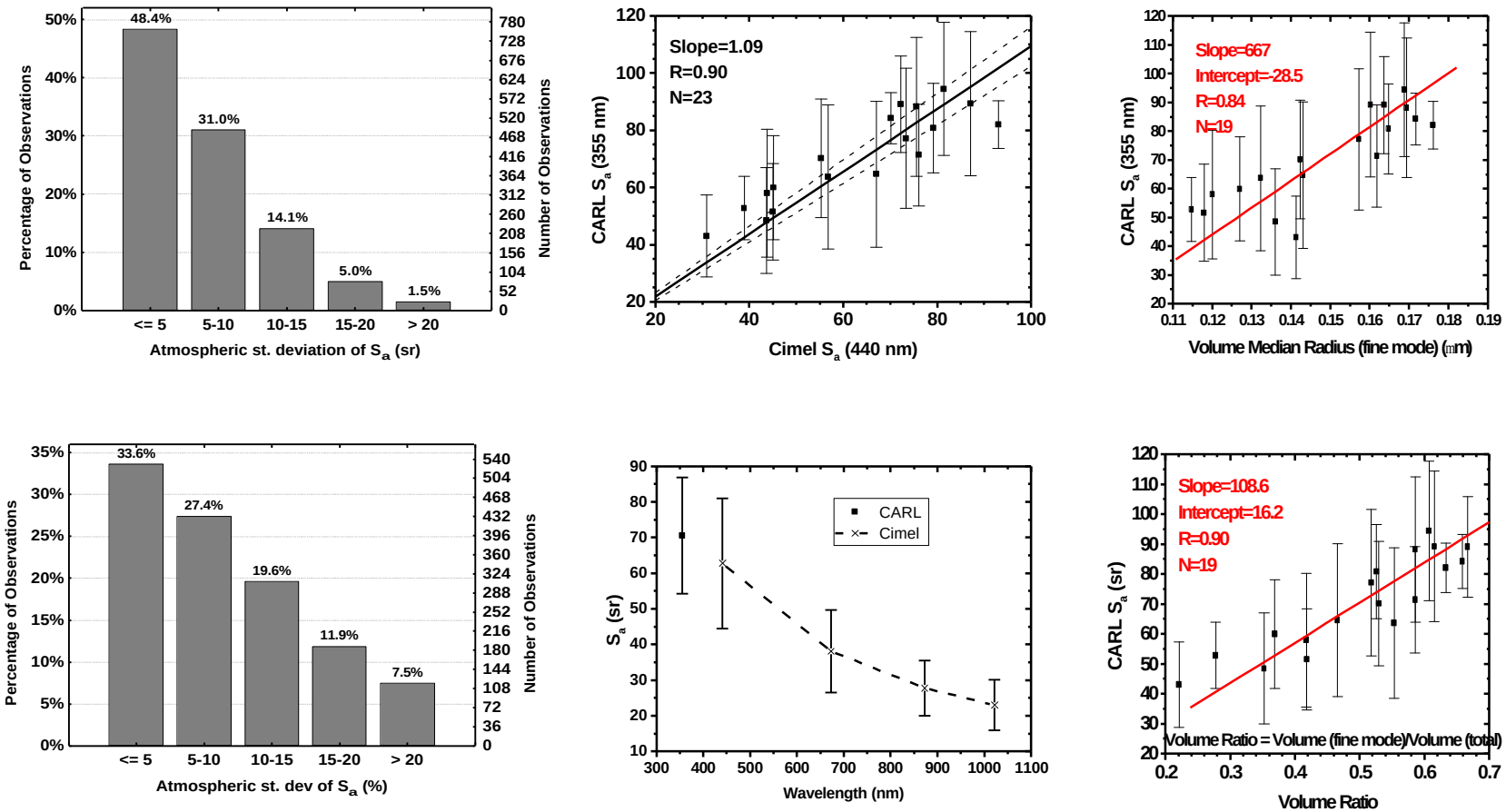

Figure 10. Standard deviation of S_a in a vertical column due to atmospheric variability for CART Raman lidar data acquired between April 1998 and April 1999. Top graph shows standard deviation in steradians and bottom graph shows this as a percentage of the measured S_a

Figure 11. (top) Comparison of S_a measured by CART Raman lidar and derived from Sun and sky radiances measured by Cimel Sun photometer. (bottom) Wavelength dependence of S_a

Figure 12. Comparison of fine mode volume mean radius (top) and volume ratio (bottom) derived by inverting Sun and sky radiances with CART Raman lidar measurements of S_a

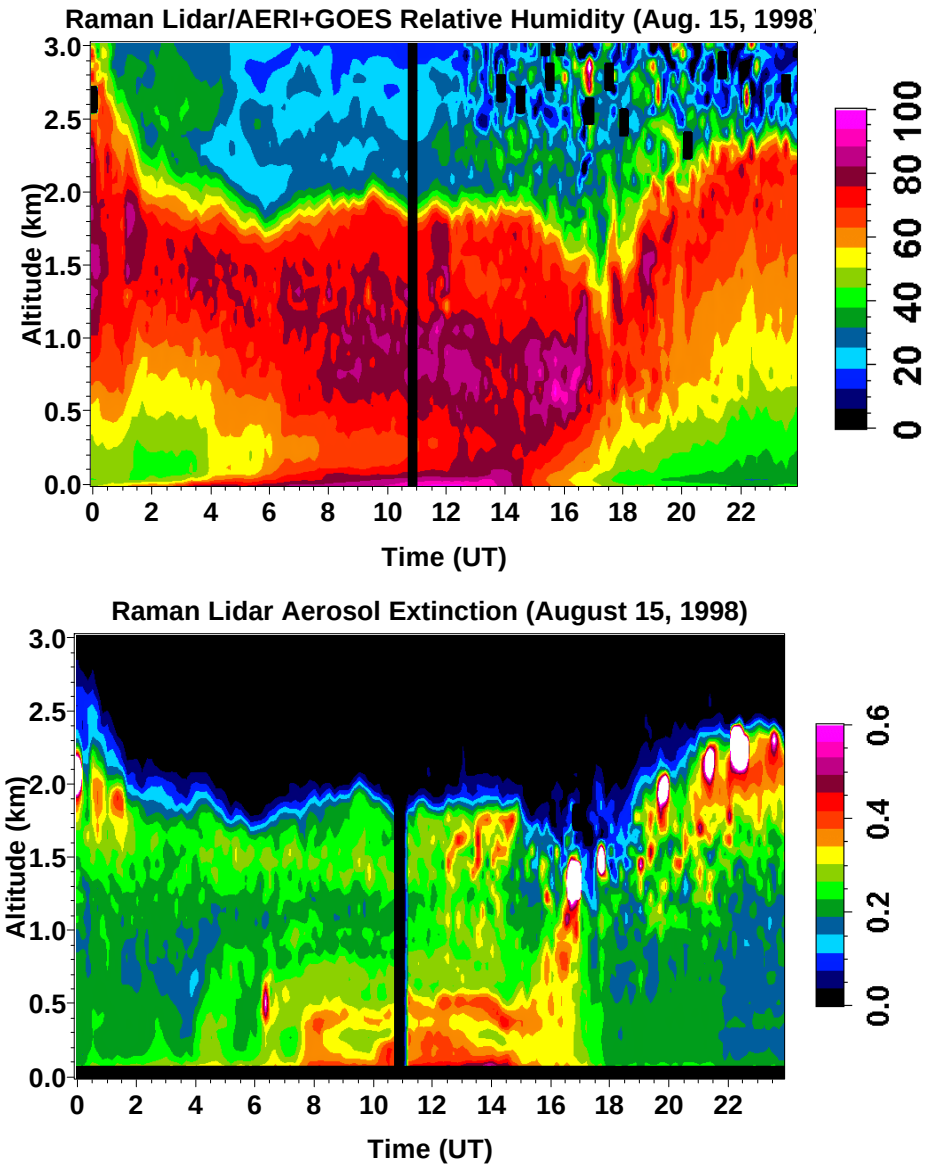

Figure 13. Images showing CART Raman lidar measurements of relative humidity (top) and aerosol extinction (bottom) on August 15, 1998

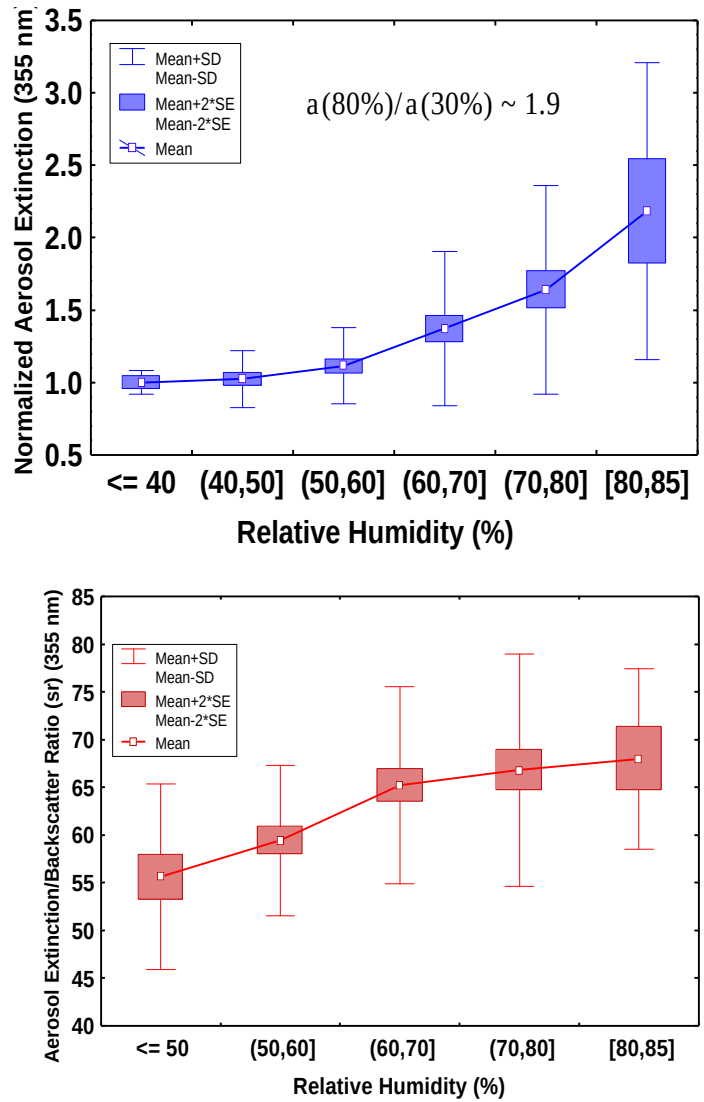

Figure 14. Average distributions of normalized aerosol extinction (top) and aerosol extinction/backscattering ratio (bottom) as a function of relative humidity for cases of hygroscopic aerosol growth near the top of the daytime boundary layer.

Mean Aerosol Extinction Profiles

- Seasonal variability in aerosol optical thickness
- Vertical distributions vary with aerosol optical thickness and season

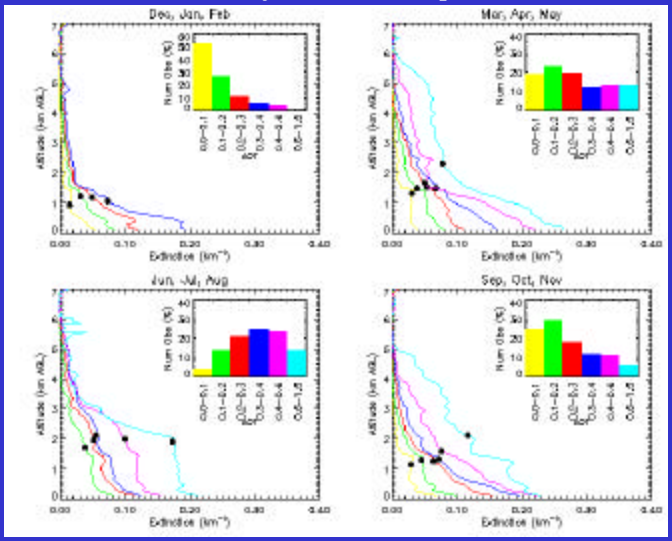

Richard Ferrare, NASA Langley Research Center, 2000

The Raman lidar aerosol extinction profiles have been used to examine the vertical variability of aerosols. This figure shows the average aerosol extinction profiles for various ranges of AOT for data acquired between April 1998 to January 2000. The histograms show the distribution of aerosol optical thickness for each season. The solid points on this graph indicate the scale height of the aerosols. The aerosol scale height was between 1.0-1.2 km during the winter but rose to nearly 2 km in the summer. This behavior is in contrast to the scale height for water vapor mixing ratio, which remained nearly the same (2.0-2.5 km) during winter and summer. The Raman lidar aerosol extinction profiles also show that considerable aerosol loading often existed in elevated layer above the boundary layer.

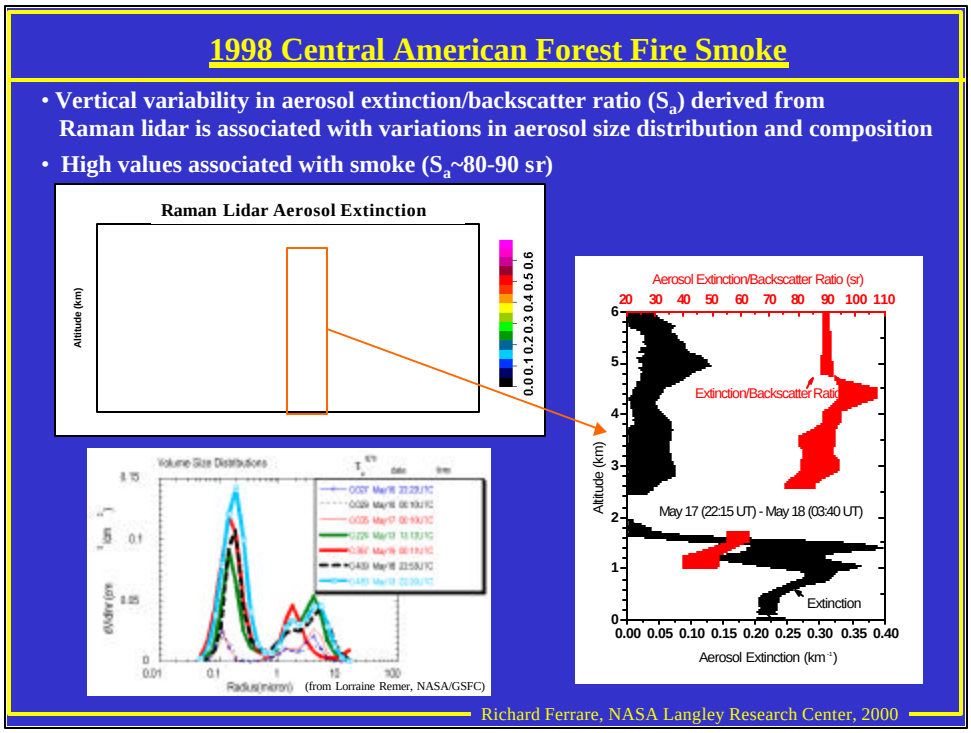

The CART Raman Lidar (CARL) aerosol extinction profiles also show that considerable aerosol loading often existed in elevated layer above the boundary layer. This figure shows an example when smoke from fires in Central America were observed over the SGP site. Of particular importance in this case is the profile of the aerosol extinction/backscatter ratio (S_a) derived from the CARL data and which is also shown in this figure. Since S_a varies with changes in the aerosol size distribution and/or aerosol composition, variations in the vertical profile of S_a indicate that the aerosol size distribution and/or aerosol composition varied with altitude. In this example, the value of S_a = 55 sr observed for the boundary layer aerosols is typical of the aerosols observed over the SGP site. In contrast, the value of S_a = 90 sr observed for the elevated aerosol layer between 3-6 km is typical for biomass burning aerosols. We used aerosol size distributions derived from the Cimel Sun photometer sun and sky radiance measurements to show that the biomass burning aerosols are consistent with the CARL S_a measurements.